Real-Time Obstacle Avoidance for Continuum Manipulator: Towards Safer Application in Human Environments

Ahmad Ataka, Ali Shafti, Ali Shiva, Helge Wurdemann, and **Kaspar Althoefer**
Centre for Robotics Research, King's College London
Strand, London, WC2R 2LS
England, United Kingdom

Abstract

The rigid-link manipulators have been extensively employed in industrial setting nowadays. However, problem arises when such manipulators are assigned to work alongside human or employed in cluttered, complex, and tight environment. Hence, continuum manipulator, with its inherent compliant and flexibility, is preferable in this aspect. In this paper, we present our recent work presenting a real-time pose estimation and obstacle avoidance for continuum manipulator in dynamic environments. The approach is shown to work in a model of both single-segment and multi-segment continuum manipulator and also in a real tendon-driven single-segment continuum manipulator in dynamic environment, and thus, suitable to be used in human environments.

Introduction

Nowadays, the field of rigid-link manipulators is a well-established discipline. Its ability to have precise position control and trajectory generation for doing various manipulations and tasks has made it popular in industrial setting. The rigid-link manipulators are now used daily in various industrial environment and manufacturing plants worldwide. However, the current generation of rigid-link manipulators are mainly employed automatically in task with limited human intervention due to the safety reason. This constraints the applicability of such manipulators to tasks which require human-robot collaboration.

Several researchers proposed solutions for safer human-robot interaction, such as the utilization of flexible joint (Ozgoli and Taghirad 2006) and variable stiffness actuator (Kim and Song 2010), an elastic strip approach which exploits redundancy of the manipulators (Khatib et al. 1999), (Brock and Khatib 2002), and others which include safety criteria to robots motion planning and obstacle avoidance (Haddadin et al. 2013). These, however, do not eliminate the fact that most industrial manipulators still need an open space and well-defined environment in order to execute the task.

One alternative solution is by employing a continuum-style manipulators, mainly used in medical applications (Burgner-Kahrs, Rucker, and Choset 2015). Mostly inspired by nature, such as octopus arm (McMahan et al. 2006) or snake (Hirose 1993), continuum manipulator has an ability to bend at any point along its body. Thus, it is very suitable to be used in complex and tight environments where the rigid-link counterparts would be unable to manoeuvre. Its inherent compliance will also make it safer and more adaptable when interact with sensitive environment, including human. Continuum manipulators, for example mounted on mobile platforms, will have more flexibility than their rigid-link counterparts when employed in industrial setting with human presence.

Figure 1: A tendon-driven single-segment arms used as a model in this paper. To measure the tip's pose and the obstacle's pose, the NDI Aurora tracker can be adopted.

However, the advantage of backbone flexibility possessed by continuum manipulators comes with the consequence of difficulty in modelling their structure. This will in turn complicates the motion planning and trajectory generation. The model-based pose estimator is needed to correctly estimate the pose of manipulators body such that the real-time obstacle avoidance can be employed to safely avoid collision with human or dynamic environments.

In this paper, we present a real-time obstacle avoidance for continuum manipulators in dynamic environments. The obstacle avoidance is equipped with non-linear observer to estimate the pose of any point along the body of manipu-

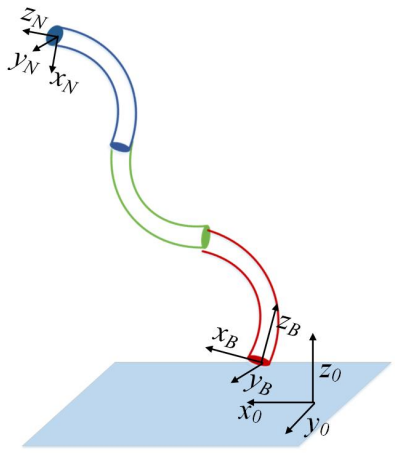

Figure 2: An illustration of three segments continuum manipulator with mobile base.

lator to make sure that the whole body of the manipulator can avoid collision. The algorithm is tested for a model of tendon-driven single-segment continuum manipulator as shown in Figure 1 and has been verified experimentally as presented in (Ataka et al. 2016). The obstacle avoidance is also implemented to a model of multi-segment continuum manipulators with mobile platform (Ataka et al. 2016). The overall algorithm is shown to work well in avoiding moving obstacle, and thus, makes it suitable to be used in human environments.

Continuum Manipulator

Kinematic Model

Here, we present a model of a tendon-driven continuum manipulator. The manipulator is moved by modifying the length of three uniformly distributed tendons along the surface in each segment The model is based on constant-curvature assumption, i.e. each segment is assumed to have a constant radius of curvature at a given time. Each segment can then be parameterized by configuration space variables $\mathbf{k}_i$ consisting of curvature κ_i, deflection angle ϕ_i, and segment length s_i. The forward kinematics relation mapping these variables to task space position of the segments tip is presented in (Webster and Jones 2010). For a continuum manipulator with mobile platform, as shown in Figure 2, the homogeneous transformation of the end-effector with respect to the world frame is expressed as

$$ {}^{N}_{0}\mathbf{T}(\mathbf{k}) = \mathbf{T}_B \prod_{i=1}^{N} {}^{i}_{i-1}\mathbf{T}(\mathbf{k}_i) \tag{1} $$

Where N specifies the segment number, $\mathbf{k} = [\mathbf{k}_1 \quad \mathbf{k}_2 \quad \dots \quad \mathbf{k}_N]^T$ denotes the vector consisting of configuration space variables of all segments, and $\mathbf{T}_B \in SE(3)$ denotes the homogeneous transformation matrix of the frame attached to the base.

Moreover, the mapping from the configuration space variables $\mathbf{k}$ to the actuator space $\mathbf{q}$, in this case specifies tendons length, is also well defined in (Webster and Jones 2010). Adding the mobile platform pose $\mathbf{q}_0$ to the actuator space $\mathbf{q}$, we have $\mathbf{q} = [\mathbf{q}_0 \quad \mathbf{q}_1 \quad \dots \quad \mathbf{q}_N]^T$ where each component $\mathbf{q}_i$ consists of the tendon length of each segment, written as $\mathbf{q}_i = [l_{i1} \quad l_{i2} \quad l_{i3}]^T$.

In order to specify any point along the body of the manipulator, we use a scalar $\xi_i \in [0,1]$ for each segment, ranging from the base ($\xi_i = 0$) to the tip ($\xi_i = 1$). The list of scalars ξ_i for all segments are then combined to be a vector ξ whose value is govern by $\xi = \{\xi_r = 1 : \forall r < i, \xi_i, \xi_r = 0 : \forall r > i\}$.

In short, we can write the forward kinematics of the continuum manipulators as

$$ {}^{N}_{0}\mathbf{T}(\mathbf{q},\xi) = \begin{bmatrix} \mathbf{R}(\mathbf{q},\xi) & \mathbf{p}(\mathbf{q},\xi) \\ \mathbf{0}_{1\times 3} & 1 \end{bmatrix} \tag{2} $$

where $\mathbf{R}(\mathbf{q},\xi) \in SO(3)$ stands for the rotation matrix and $\mathbf{p}(\mathbf{q},\xi) \in \mathbb{R}^3$ stands for the position vector of the point along the body of manipulator. The Jacobian for our kinematic model, defined as $\mathbf{J}(\mathbf{q},\xi) = \frac{\partial \mathbf{p}(\mathbf{q},\xi)}{\partial \mathbf{q}} \in \mathbb{R}^{3\times(3N+6)}$, is expressed as follows

$$ \dot{\mathbf{p}}(\mathbf{q},\xi) = \mathbf{J}(\mathbf{q},\xi)\dot{\mathbf{q}} \Leftrightarrow \dot{\mathbf{q}} = \mathbf{J}(\mathbf{q},\xi)^{-1}\dot{\mathbf{p}}(\mathbf{q},\xi). \tag{3} $$

State-Space Representation

The kinematic model can also be expressed in terms of state space representation, i.e. the state equation and output equation. Here, we present the state space analysis for a static single segment only. We use the tendon length $\mathbf{q} \in \mathbb{R}^3$ as our state, $\mathbf{x} \in X$. Hence, the input to our system, $\mathbf{u} \in U$, is given by the actuator lengths rate of change, $\dot{\mathbf{q}} \in \mathbb{R}^3$, which is governed by DC motors connected to the tendon. The measurement value $\mathbf{y}_k \in Y$ comes from a position sensor embedded in the tip of manipulator. The NDI Aurora tracker, like the one shown in Figure 1, can be used for this purpose. Hence, the output equation matches the component of the matrix given by the forward kinematics relation in 2, $\mathbf{p}(\mathbf{q},\xi)$ for $\xi = 1$ (tip). Here, X, U, and Y denote the state space, input space, and output space respectively.

The state space and output equation in discrete form, for a sampling time of Δt, can then be expressed as

$$ \mathbf{x}_{k+1} = f(\mathbf{x}_k, \mathbf{u}_k) = \mathbf{x}_k + \Delta t \mathbf{u}_k. \tag{4} $$

$$ \mathbf{y} = g(\mathbf{x}_k) = \mathbf{p}(\mathbf{q}, \xi = 1), \tag{5} $$

where the function $f : X \times U \to X$ is used to map the current state and input to the next state while $g : X \to Y$ is used to map the current state to the output.

However, using only this information is not enough to estimate the pose of the whole body of the manipulator, due to the unknown initial state value. This is where the non-linear observer is needed to estimate the state and, in turn, use the estimation state to estimate the pose of any point along the body of manipulators.

Pose Estimation and Obstacle Avoidance

Pose Estimation

Based on the presented state space model, we employ a well-known Extended Kalman Filter (EKF) approach to our

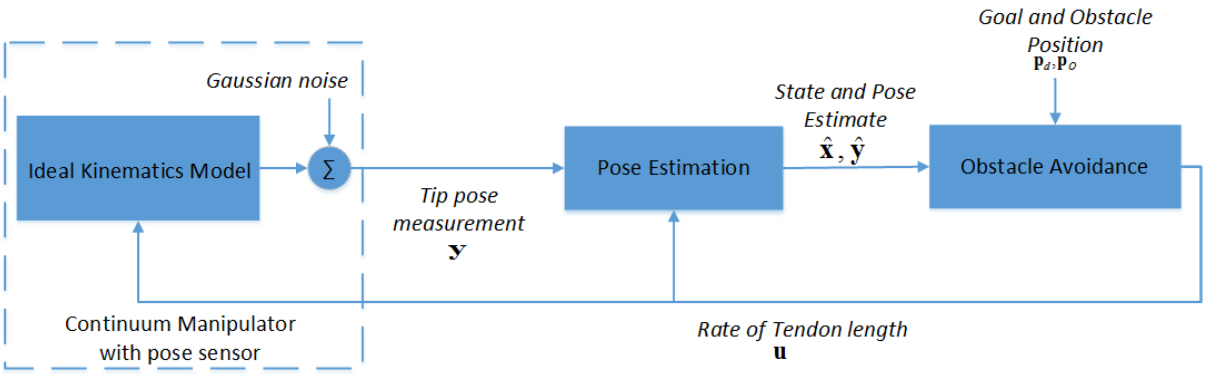

Figure 3: The proposed pose estimator and obstacle avoidance algorithm. An ideal kinematics model, added with Gaussian noise, is used to replace the continuum manipulator and the pose sensor during the simulation.

model. The EKF can be formulated as

$$\begin{aligned}
\hat{\mathbf{x}}_{k+1|k} &= f(\hat{\mathbf{x}}_{k|k}, \mathbf{u}_k), \\
\mathbf{P}_{k+1|k} &= \mathbf{A}_k \mathbf{P}_{k|k} \mathbf{A}_k^T + \mathbf{Q}_k, \\
\mathbf{K}_k &= \mathbf{P}_{k+1|k} \mathbf{C}_k^T (\mathbf{C}_k \mathbf{P}_{k+1|k} \mathbf{C}_k^T + \mathbf{R}_k)^{-1}, \\
\hat{\mathbf{x}}_{k+1|k+1} &= \hat{\mathbf{x}}_{k+1|k} + \mathbf{K}_k (\mathbf{y}_k - g(\hat{\mathbf{x}}_{k+1|k})), \\
\mathbf{P}_{k+1|k+1} &= (\mathbf{I} - \mathbf{K}_k \mathbf{C}_k) \mathbf{P}_{k+1|k}.
\end{aligned} \tag{6}$$

$\hat{\mathbf{x}}_{k+1|k+1}$, $\hat{\mathbf{x}}_{k|k}$, $\mathbf{u}_k$, and $\mathbf{y}_k$ represent the next state estimation, the current state estimation, the input signal, and the measurement data respectively. The matrix $\mathbf{Q}_k \in \mathbb{R}^{3\times3}$ and $\mathbf{R}_k \in \mathbb{R}^{3\times3}$ are the process noise variance and measurement noise variance respectively.

The matrix $\mathbf{A}_k$ and $\mathbf{C}_k$ are defined as $\mathbf{A} = \frac{\partial f(\mathbf{x}_k, \mathbf{u}_k)}{\partial \mathbf{x}_k}$, $\mathbf{B} = \frac{\partial f(\mathbf{x}_k, \mathbf{u}_k)}{\partial \mathbf{u}_k}$ and $\mathbf{C} = \frac{\partial g(\mathbf{x}_k)}{\partial \mathbf{x}_k}$ respectively and can be written as

$$\mathbf{A}_k = \frac{\partial f(\mathbf{x}_k, \mathbf{u}_k)}{\partial \mathbf{x}_k} = \mathbf{I} \in \mathbb{R}^{3\times3}, \tag{7}$$

$$\mathbf{C}_k = \frac{\partial g(\mathbf{x}_k)}{\partial \mathbf{x}_k} = \frac{\partial \mathbf{p}(\mathbf{q}_k, \xi = 1)}{\partial \mathbf{q}_k} = \mathbf{J}(\mathbf{q}_k, \xi = 1). \tag{8}$$

The estimation state can then be used to estimate the pose of any point along the body of manipulator using a forward kinematics relation in (2) by modifying the scalar ξ from 0 (base) to 1 (tip). This information is used in the obstacle avoidance stage.

Modified Potential Field

The reactive potential field presented in (Khatib 1985) is modified here. The idea is to use the potential function U to attract the tip of manipulator to a desired target position and repel its body from colliding with environment. A standard potential field, which usually produces a task space force $\mathbf{F} = -\nabla U$, is modified such that it is suitable to be used in continuum manipulators kinematic model. Rather than force, the task space velocity $\dot{\mathbf{p}}$ is produced.

The attractive potential field is given by

$$\dot{\mathbf{p}}_{\mathbf{p}_d} = -c(\mathbf{p} - \mathbf{p}_d). \tag{9}$$

where $\mathbf{p}_d$ and c represent desired position and a positive constant gain respectively. The repulsive field is expressed as

$$\dot{\mathbf{p}}_{\mathscr{O}} = \begin{cases} \eta(\frac{1}{\rho} - \frac{1}{\rho_0}) \frac{1}{\rho^2} \frac{\partial \rho}{\partial \mathbf{p}} & \text{if } \rho < \rho_0 \\ 0 & \text{if } \rho \geq \rho_0 \end{cases}. \tag{10}$$

where $\rho = \sqrt{(\mathbf{p} - \mathbf{p}_{\mathscr{O}})^T (\mathbf{p} - \mathbf{p}_{\mathscr{O}})}$ denote the closest distance from an obstacle to the manipulator's body, η is positive constant, and ρ_0 indicates the limit distance of the potential influence.

In order to achieve safer obstacle avoidance, the repulsive potential needs to be applied not only at the tip but also at points along the body of manipulator. Therefore, we define *point subjected to potential* (PSP) as a point in the backbone of manipulator in which the repulsive potential is possible to be applied. The PSP to be chosen is the closest one to the obstacles or environments. The position of this PSP as well as the tip are all estimated by the pose estimation stage at every iteration as follows

$$\hat{\mathbf{p}}_k(\xi) = \mathbf{p}(\hat{\mathbf{x}}_{k|k}, \xi). \tag{11}$$

Finally, each attractive and repulsive velocity in task space, using their corresponding working points, are mapped to the actuator space via inverse Jacobian relation. The combined velocity in actuator space is then fed as an input to our manipulator, $\mathbf{u}_k$, as follows

$$\mathbf{u}_k = \dot{\mathbf{q}} = \mathbf{J}_e^{-1} \dot{\mathbf{p}}_{\mathbf{p}_d} + \mathbf{J}_a^{-1} \dot{\mathbf{p}}_{\mathscr{O}}, \tag{12}$$

where $\mathbf{J}_e$ and $\mathbf{J}_a$ indicate the Jacobian of the tip and the chosen PSP respectively and $\dot{\mathbf{p}}_{\mathscr{O}_b}$ represents repulsive potential produced by the closest obstacle.

The overall pose estimation and obstacle avoidance algorithm is combined as shown in Figure 3.

Mechanical Constraint Avoidance

Other problem that needs to be addressed for this kind of manipulator is the inherent mechanical limitation which can disturb the movement of the manipulator in avoiding obstacle. In a tendon-driven manipulator, the tendons length l_{ij} can only be in the region of $(1-\zeta)L < l_{ij} < (1+\zeta)L$ where

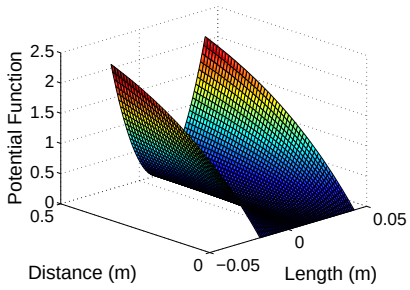

Figure 4: Illustration of the proposed potential function designed to satisfy mechanical constraint as function of the tendon's length and end-effector-to-target Euclidean distance.

ζ and L represent extension ratio and normal length respectively.

We propose an attractive potential in actuator space to attract the length towards normal length L, and thus, makes the tendons avoid mechanical constraint. The potential function is described as

$$U_{lim}(\mathbf{q}) = \sum_{i=1}^{N}\sum_{j=1}^{3}\sigma(\frac{l_{ij}-L}{\zeta L})^2, \tag{13}$$

where σ is positive constant. The attractive velocity field is as follows

$$\dot{\mathbf{q}}_{lim}(\mathbf{q}) = -2\sigma\frac{1}{\zeta^2 L^2}(\mathbf{l}-\mathbf{L}), \tag{14}$$

where $\mathbf{l} = [l_{11} \quad ... \quad l_{13} \quad l_{21} \quad ... \quad l_{N3}]^T$ and $\mathbf{L} = L\mathbf{1}_{3N\times 1}$.

Moreover, we weight this potential field by a weight function w which will reduce the contribution of the mechanical constraint field as the end effector approaches the target position, as follows

$$w(\mathbf{x}) = (1 - e^{-\mu\|(\mathbf{x}-\mathbf{x}_d)\|}), \tag{15}$$

where μ is positive constant.

Figure 4 shows an illustration of this potential as a function of tendons length as well as the distance between end-effector and the target. The final proposed mechanical constraint avoidance in actuator space is given by

$$\dot{\mathbf{q}}_{new}(\mathbf{q},\mathbf{x}) = \begin{bmatrix}\mathbf{0}_{6\times 1} \\ w(\mathbf{x})\dot{\mathbf{q}}_{lim}(\mathbf{q})\end{bmatrix} \tag{16}$$

so that the total potential is given by

$$\dot{\mathbf{q}}(\mathbf{q}) = \mathbf{J}_e(\mathbf{q})^+\dot{\mathbf{x}}_{\mathbf{x}_d}(\mathbf{x}) + \sum_{a=1}^{m}\sum_{b=1}^{n}\mathbf{J}_a(\mathbf{q})^+\dot{\mathbf{x}}_{\mathscr{O}_b}(\mathbf{x}) + \dot{\mathbf{q}}_{new}(\mathbf{q},\mathbf{x}) \tag{17}$$

Results and Discussion

Here, we present the implementation of our approach both in the simulation and the experiment. The combined pose estimation and obstacle avoidance for single segment case is tested on a model of continuum manipulator running in a real-time simulation environment. The obstacle avoidance algorithm without the pose estimation is also validated in an experiment as presented in our publication (Ataka et al. 2016). Moreover, we also applied the obstacle avoidance and mechanical constraint avoidance to a model of multi-segment continuum manipulator as presented in the same publication. A moving obstacle, assumed to be a 5-mm-radius sphere, moves at a constant speed in the surrounding of the manipulator to simulate the part of human body's movement.

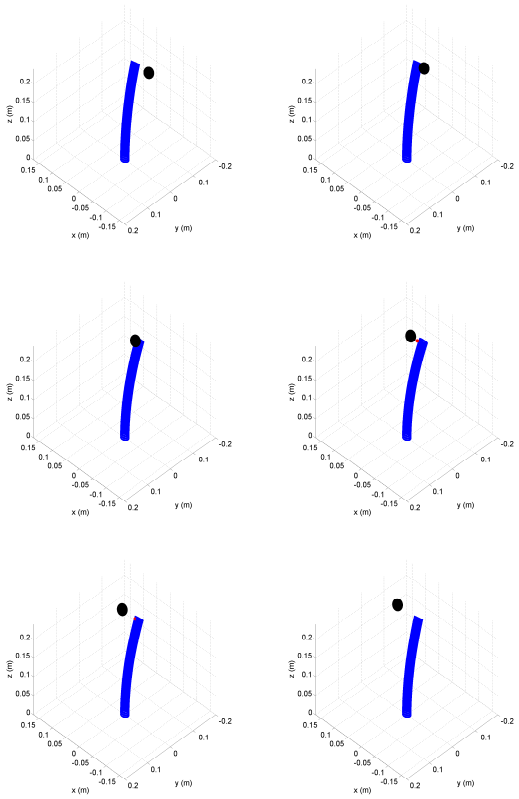

Figure 5: A single segments continuum manipulator's movement with a static target position (small red dot) when obstacle (black sphere) moves close to the tip. The order of movement is as follows: upper left picture, upper right picture, lower left picture, and finally lower right picture.

Single Segment Case

In this subsection, we will first present the simulation results of a combined pose estimation and obstacle avoidance. For the pose estimation, to simulate the sensor, an ideal kinematic model with added Gaussian noise is used. This perfect kinematic model has a true state $\mathbf{x}_k$ updated at every iteration based on the model kinematics. However, the value is assumed to be unaccessible for the obstacle avoidance, which will only capitalize the estimated states $\hat{\mathbf{x}}_k$ from the EKF. The noise has zero-mean and the standard deviation of $\sigma = 10^{-4}$. The variance matrix is then given by $\mathbf{R} = \sigma^2\mathbf{I} \in \mathbb{R}^{3\times 3}$. The black sphere represents the obstacle while the rod dot represents the tip's target, assumed to be

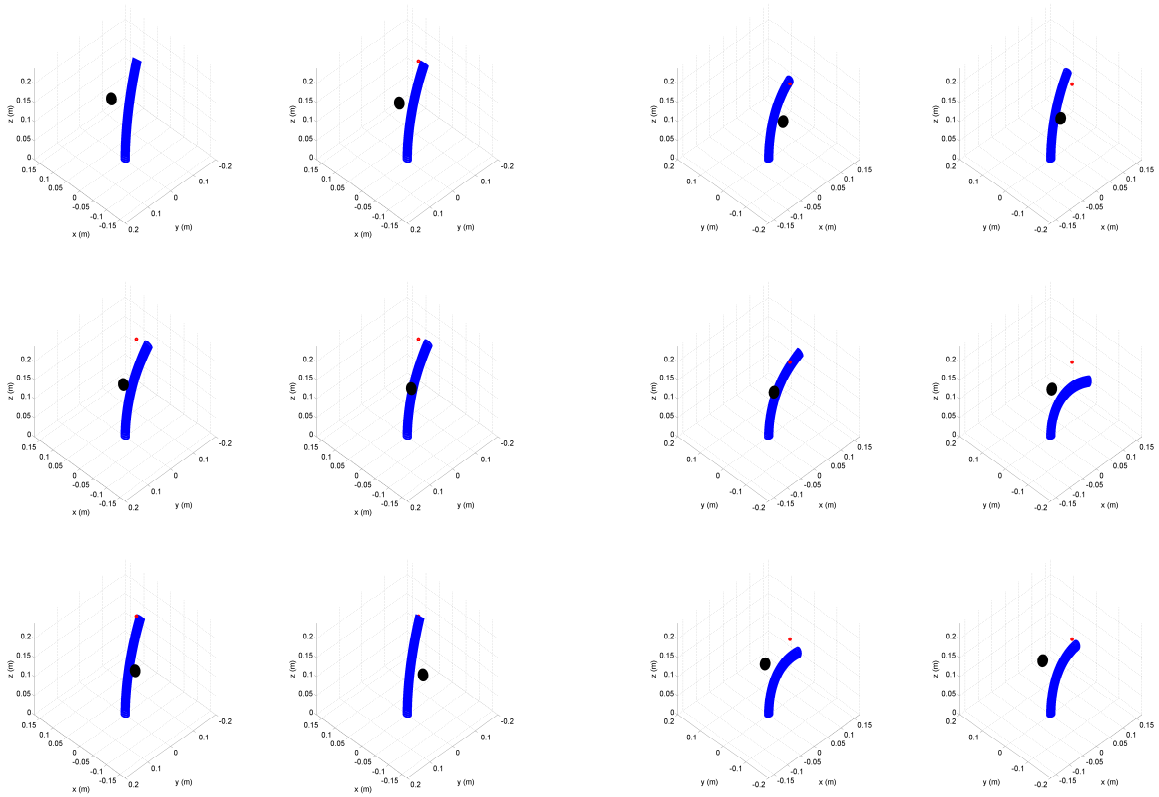

(a) (b)

Figure 6: A single segments continuum manipulator's movement with a static target position (small red dot) when obstacle (black sphere) moves close to the middle point of the manipulator's body (a) in x-axis direction and (b) y-axis direction. The order of movement for each subfigure is as follows: upper left picture, upper right picture, lower left picture, and finally lower right picture.

fixed.

We show several scenarios, such as an obstacle moves close to the segment's tip, as depicted in Figure 5 and moves close to the middle part of the backbone, as shown in Figure 6a (for the obstacle's movement in x-direction) and Figure 6b (for the obstacle's movement in y-direction). We can conclude that the proposed algorithm works well to improve the safety of the robot's body from collision. The main contribution of the algorithm, however, is demonstrated when the obstacle move at a lower height, such as in Figure 6. Our proposed algorithm enables not only the tip but also the body of manipulator to avoid obstacle.

The obstacle avoidance algorithm, without the pose estimation, has been implemented in an ortho-planar spring tendon-driven continuum manipulator as shown in Figure 1 as presented in (Ataka et al. 2016). The Maxon DC Motors are used as actuators. An electromagnetic-based Aurora sensor coil is embedded in the tip of the manipulator to track the position of the tip. The obstacle is represented by a second sensor coil hung in the air by a thread. The obstacle is assumed to be a sphere with radius of 0.01 m whose centre is specified by the second sensor coil's location. The target is assumed to move in a straight line.

We can see from Figure 7, from left to right, both the 3D view (Figure 7a) and the top view (Figure 7b) of the tip's movement, as well as the comparison between the tip-obstacle distance and the target-obstacle distance (Figure 7c). Without pose estimation, the PSP is assumed to be located only at the tip, hence, only the tip will be safe from collision.

Three Segments Case

Here, we present the performance of our proposed mechanical constraint avoidance in a model of three-segments continuum manipulator. We can see how our proposed algorithm improves the performance of continuum manipulator in tracking the moving target. Without our algorithm, once the tendons length reach their limit, there appears an immediate reduction in the manipulator's maneuverability such that the tip is unable to reach the moving target, as shown in Figure 8a. While, using our algorithm, it is shown in Figure 8b that the manipulator's tip is able to track the moving tar-

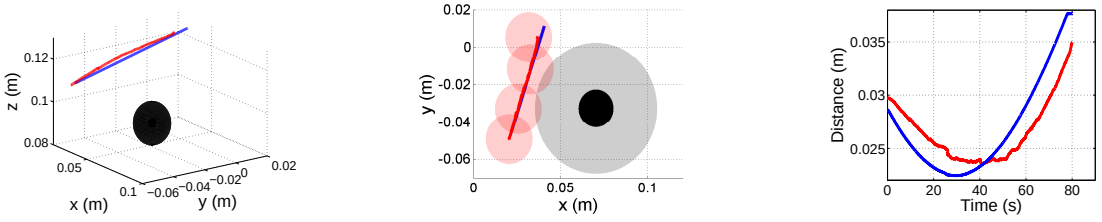

(a) (b) (c)

Figure 7: The manipulator's tip (red line) tracks the desired trajectory (blue line) and avoids static obstacle (black spheres) nearby in (a) 3D view and (b) top view. (c) The graph shows the closest distance from the obstacle to the estimated manipulator's body (red line) and to the target (blue line) respectively.

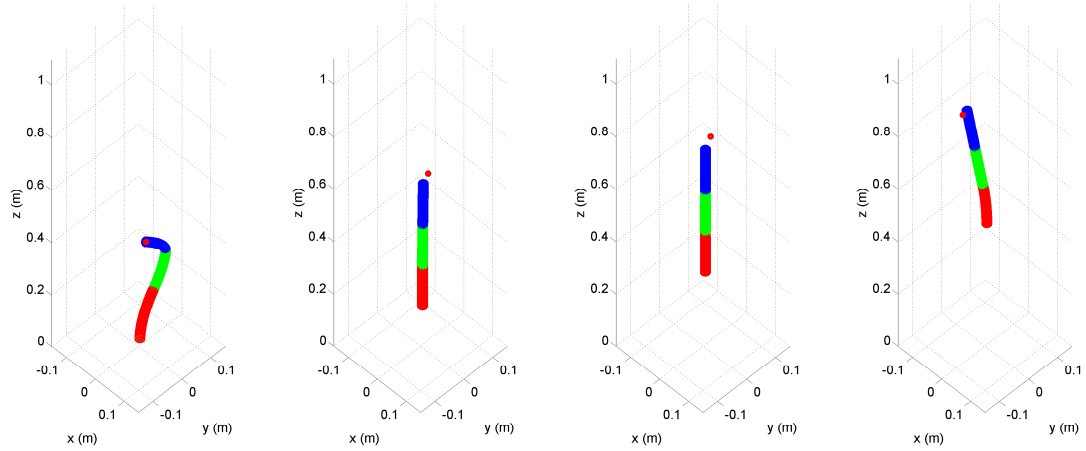

(a)

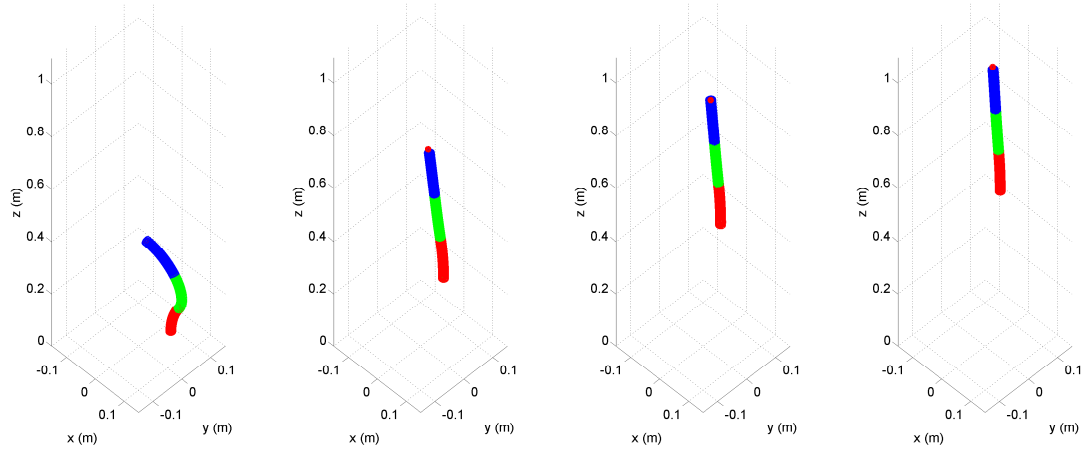

(b)

Figure 8: The movement comparison between the continuum manipulator (a) without the proposed algorithm and (b) with the proposed algorithm.

get smoothly. The complete obstacle avoidance simulation results can be seen in (Ataka et al. 2016).

Conclusions and Future Works

In this paper, we present our works on real-time obstacle avoidance, based on modified potential field, for continuum manipulators in dynamic environments. The obstacle avoidance can be equipped with a pose estimator, based on an Extended Kalman Filter, to make the whole body of manipulator safer from collision. The novel potential field in actuator space is also proposed in order to avoid the inherent mechanical constraint of the manipulators. The combined obstacle avoidance and pose estimator is shown to perform well in a simulation for the model of tendon-driven single-segment continuum manipulator. The proposed potential field is also verified in experiment. The extension of the obstacle avoidance for multi-segment case as well as the mechanical constraint avoidance is implemented successfully in a model of three-segments continuum manipulator.

The proposed algorithm has a promising capability to be implemented in a real environment consisting human. For the future works, the whole algorithm can be fully implemented for the real multi-segment continuum manipulators equipped with electromagnetic-based position sensors. The experiment to test the whole algorithm in a continuum manipulator with mobile platform will also be investigated in the future.

Acknowledgement

The work described in this paper is partially supported by the STIFF-FLOP project grant from the European Communities Seventh Framework Programme under grant agreement 287728, the Four By Three grant from the European Framework Programme for Research and Innovation Horizon 2020 under grant agreement no 637095, and the Indonesia Endowment Fund for Education, Ministry of Finance Republic of Indonesia.

References

Ataka, A.; Qi, P.; Liu, H.; and Althoefer, K. 2016. Accepted. Real-Time Planner for Multi-segment continuum manipulator in dynamic environments. *Proceedings of 2016 IEEE International Conference on Robotics and Automation (ICRA)*.

Brock, O., and Khatib, O. 2002. Elastic strips: A framework for motion generation in human environments. *The International Journal of Robotics Research* 21(12):1031–1052.

Burgner-Kahrs, J.; Rucker, D. C.; and Choset, H. 2015. Continuum Robots for Medical Applications: A Survey. *IEEE Transactions on Robotics* 31(6):1261–1280.

Haddadin, S.; Parusel, S.; Belder, R.; and Albu-Schffer, A. 2013. Computer Safety, Reliability, and Security: 32nd International Conference, SAFECOMP 2013, Toulouse, France, September 24-27, 2013. Proceedings. Berlin, Heidelberg: Springer Berlin Heidelberg. 202–215.

Hirose, S. 1993. *Biologically inspired robots: snake-like locomotors and manipulators*. Oxford science publications. Oxford University Press.

Khatib, O.; Yokoi, K.; Brock, O.; Chang, K.; and Casal, A. 1999. Robots in human environments. In *Robot Motion and Control, 1999. RoMoCo '99. Proceedings of the First Workshop on*, 213–221.

Khatib, O. 1985. Real-time obstacle avoidance for manipulators and mobile robots. In *Robotics and Automation. Proceedings. 1985 IEEE International Conference on*, volume 2, 500–505.

Kim, B. S., and Song, J. B. 2010. Hybrid dual actuator unit: A design of a variable stiffness actuator based on an adjustable moment arm mechanism. In *Robotics and Automation (ICRA), 2010 IEEE International Conference on*, 1655–1660.

McMahan, W.; Chitrakaran, V.; Csencsits, M.; Dawson, D.; Walker, I.; Jones, B.; Pritts, M.; Dienno, D.; Grissom, M.; and Rahn, C. 2006. Field trials and testing of the OctArm continuum manipulator. In *Robotics and Automation, 2006. ICRA 2006. Proceedings 2006 IEEE International Conference on*, 2336–2341.

Ozgoli, S., and Taghirad, H. 2006. A survey on the control of flexible joint robots. *Asian Journal of Control* 8(4):332–344.

Webster, III, R. J., and Jones, B. A. 2010. Design and Kinematic Modeling of Constant Curvature Continuum Robots: A Review. *Int. J. Rob. Res.* 29(13):1661–1683.